Journal of Alloys and Compounds 469 (2009) 512–518

Journal of ALLOYS AND COMPOUNDS

www.elsevier.com/locate/jallcom

Influence of cold deformation on martensite transformation and mechanical properties of Ti–Nb–Ta–Zr alloy

Liqiang Wang, Weijie Lu *, Jining Qin, Fan Zhang, Di Zhang

State Key Laboratory of Metal Matrix Composites, Shanghai Jiao Tong University, Shanghai 200240, PR China

Received 21 October 2007; received in revised form 26 January 2008; accepted 2 February 2008
Available online 24 March 2008

Abstract

Ti–35Nb–2Ta–3Zr alloy was fabricated by vacuum consumable arc melting furnace and hot pressing. Microstructure and phase transformation of solution-treated (ST) and cold-rolled (CR) plates of Ti–Nb–Ta–Zr alloy were observed. Different microstructure of strain-induced martensite transformation during cold deformation were investigated. With the increase of reduction of cold rolling, microstructure of α''-phase changed from acicular martensite to butterfly shaped martensite and showed variant crossed and cross-hatched when the reduction of cold rolling was over 60%. Mechanical properties and SEM images of the fracture surface indicated that the alloy fabricated by cold deformation showed favorable strength and plasticity. Owing to the excellent cold workability and biomedical safety of elements of Nb, Ta and Zr, Ti–Nb–Ta–Zr alloy contributed much to medical applications.

Keywords: Phase transitions; Microstructure; Mechanical properties; X-ray diffraction; Scanning electron microscopy

1. Introduction

Titanium and its alloys have been widely used as materials for biomedical applications for many years. By now, Ti–Ni alloys have been successfully applied for many medical products for a long time. Because of Ni-hypersensitivity and cytotoxicity of Ni, new kinds of Ni-free titanium alloys have been developed [1–3]. Kawahara reported that metallic Ti, Nb, Zr, Pd and Ta were low cytotoxic elements [4–7]. Therefore, new types of β titanium alloys including the elements of Nb, Zr, Pd and Ta are being studied as biomedical titanium alloys [8,9]. Recently, according to Morinaga's study, a new method for alloy design on the basis of the molecular orbital calculation of electronic structures has been proposed [10]. Those β titanium alloys such as Ti–Nb, Ti–Ta and Ti–Zr, which show high strength and low elastic modulus have been developed [11–13].

By now, many studies referring to the microstructure of strain-induced martensite transformation of NiTi alloys have been investigated for many years. However, few reports are focusing on strain-induced martensite transformation of β titanium alloys. It is known that most β titanium alloys possess excellent ability of cold deformation. A new β-type biomedical titanium alloy, Ti–Nb–Ta–Zr, which shows good cold workability is studied in this paper. The purpose of this study is to investigate the effect of cold deformation on martensite transformation and mechanical properties.

2. Experimental procedure

The Ti–Nb–Ta–Zr alloy with a nominal composition of Ti–35Nb–2Ta–3Zr (wt%) was fabricated by vacuum consumable arc melting furnace. The ingot was re-melted three times to ensure compositional homogeneity. The alloy ingot was homogenized at 1223 K for 3.6 ks in vacuum condition and then forged into a quadrate casting of 70 mm width × 30 mm thickness × 100 mm length. Followed by solution heat treatment for 0.5 h at 1053 K, the alloy was cold-rolled (CR) with the reductions of 20%, 40%, 60% and 80% in thickness. All specimens were prepared from the cold-rolled sheets by cutting, grinding and polishing. Microstructure observations were carried out by optical microscope and field emission scanning electron microscope (SEM). The transmission electron microscopy (TEM) observation was conducted using a JEM-2000EX operated at 160 kV. The temperature of martensite transformation was measured by differential scanning calorimetry (DSC) at a heating or cooling rate of 10 K/min. X-ray diffraction measurements were carried out at room temperature under the conditions of Cu Kα, 35 kV, and 100 mA. Tensile tests were carried out at a strain rate of 1.5×10^{-4} s at room temperature.

* Corresponding author. Tel.: +86 21 34202461; fax: +86 21 34202749.
E-mail address: luweijie@sjtu.edu.cn (W. Lu).

0925-8388/$ – see front matter © 2008 Elsevier B.V. All rights reserved.
doi:10.1016/j.jallcom.2008.02.032

3. Results and discussion

3.1. Microstructure analysis

Fig. 1 shows the microstructure of solution-treated (ST) specimen and cold-rolled specimens with the reductions of 20%, 40%, 60% and 80%. Seen from Fig. 1(a), no trace of martensite and α-phase were seen in the image of solution-treated specimen. Microstructure was assigned to an equiaxial β-phase. As for Ti–Nb phase diagram (Fig. 2), the temperature of $\alpha + \beta \rightarrow \beta$ transformation was much lower than 1053 K when the content of Nb was around 35 wt%. The cooling processing was so rapid that α-phase precipitation was not indicated when Ti–35Nb–2Ta–3Zr alloy was quenched quickly at 1053 K.

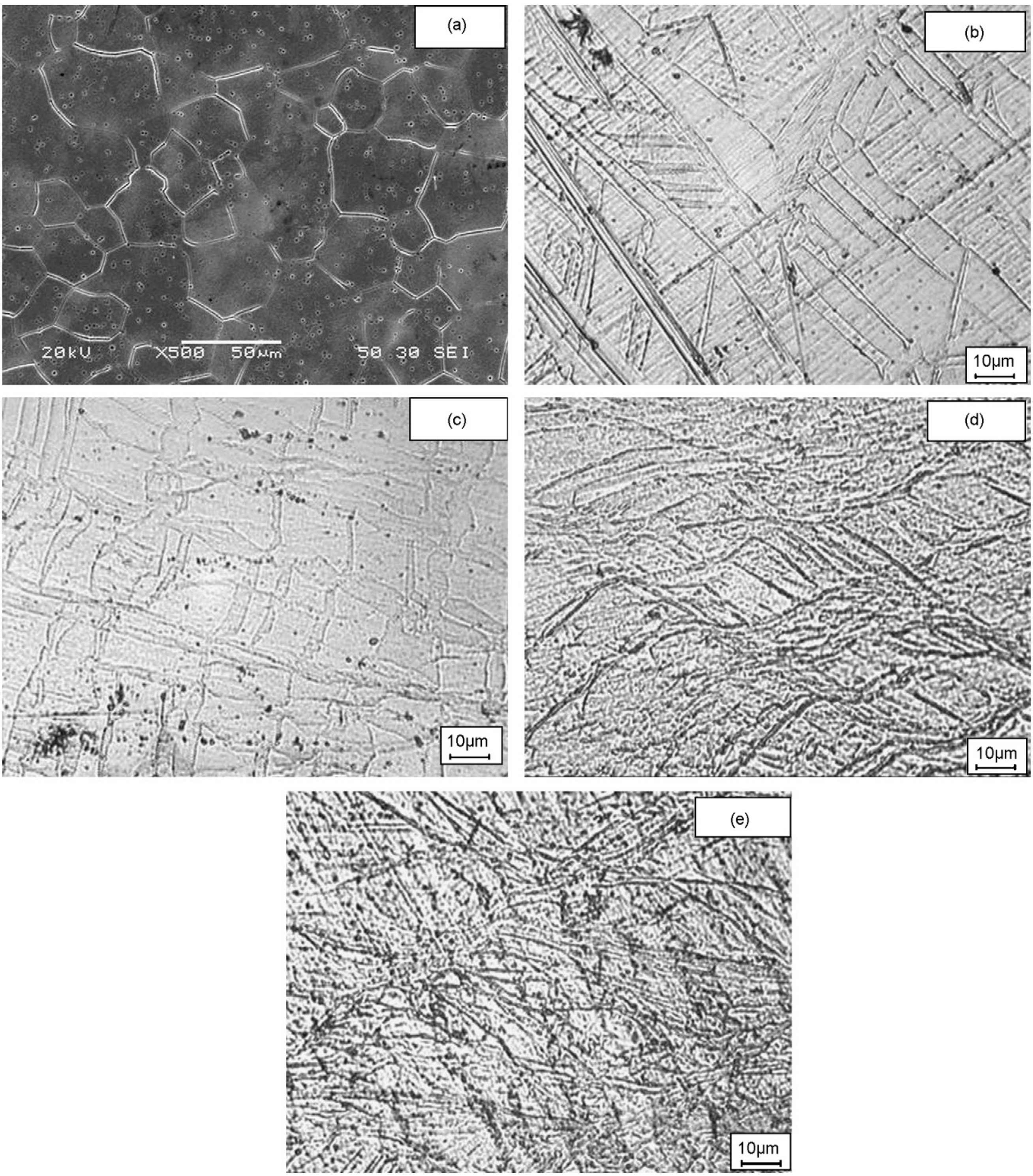

Fig. 1. Microstructure of solution-treated specimen at 1053 K for 0.5 h (a) and cold-rolled specimens with the reductions of 20% (b), 40% (c), 60% (d) and 80% (e).

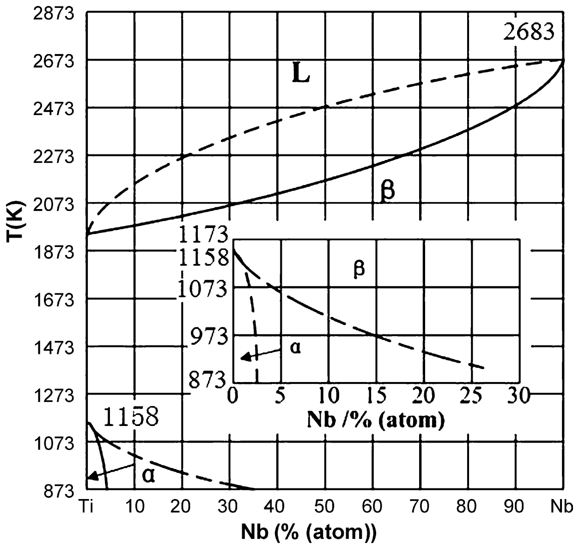

Fig. 2. Ti–Nb phase diagram [14].

Fig. 3 shows the pseudo-binary diagram of titanium with the decomposition products of the β-phase. As it shows, with the increase of the content of β-stabilizing element such as Nb, the start temperature of martensite transformation (M_s) decreased gradually. Fig. 4 shows the DSC curve of solution-treated Ti–35Nb–2Ta–3Zr alloy. Clear peaks of martensite transformation were seen during the process of heating and cooling. The M_s was measured around 199.7 K–197.5 K and the finished temperature of martensite transformation (M_f) was estimated around 170.1 K–169.9 K. Much more β-stabilizer Nb decreased the M_s, so there would be no martensite when the alloy was cooled to room temperature during solid solution treatment, which was consistent with the microstructure of solution-treated specimen in Fig. 1(a).

When the alloy was cold-rolled, strain-induced martensite transformation from β to α″ (orthorhombic) appeared. When the alloy was rolled by 20% in thickness, strain-induced α″ martensite was visible. Acicular α″ martensite caused by cold deformation was apparent (Fig. 1(b)). Much butterfly shaped

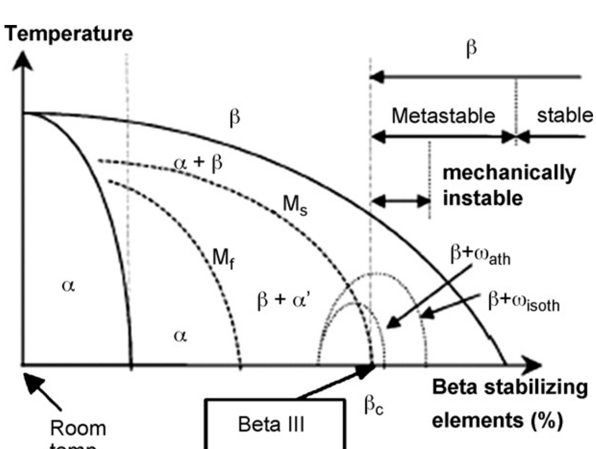

Fig. 3. Pseudo-binary diagram of titanium with the decomposition products of the β-phase [15].

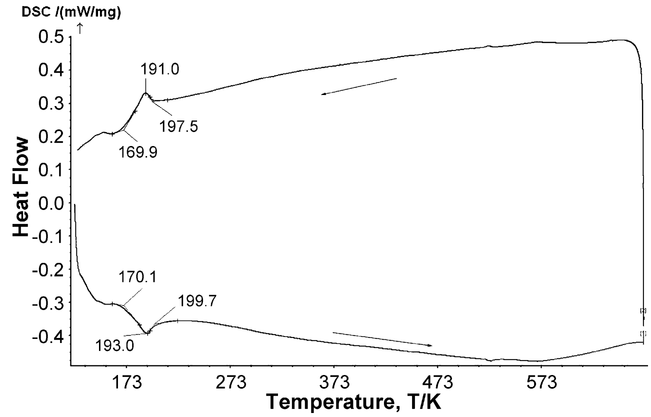

Fig. 4. DSC curve of solution-treated Ti–35Nb–2Ta–3Zr alloy.

martensite was indicated in the alloy with reduction of 40%, shown in Fig. 1(c). There was a little difference in surface microstructure of martensite during different reduction of cold rolling. With the increase of the reduction of cold rolling, much variant crossed martensite tending to rolling direction could be seen easily (Fig. 1(d)). When the alloy was rolled by 80% reduction in thickness, variant crossed martensite grew up and much more fibriform martensite appeared along rolling direction (Fig. 1(e)). The TEM of strain-induced martensite of the specimen rolled by 80% is showed in Fig. 5. As the white arrows show, the secondary microstructure of martensite exhibited as

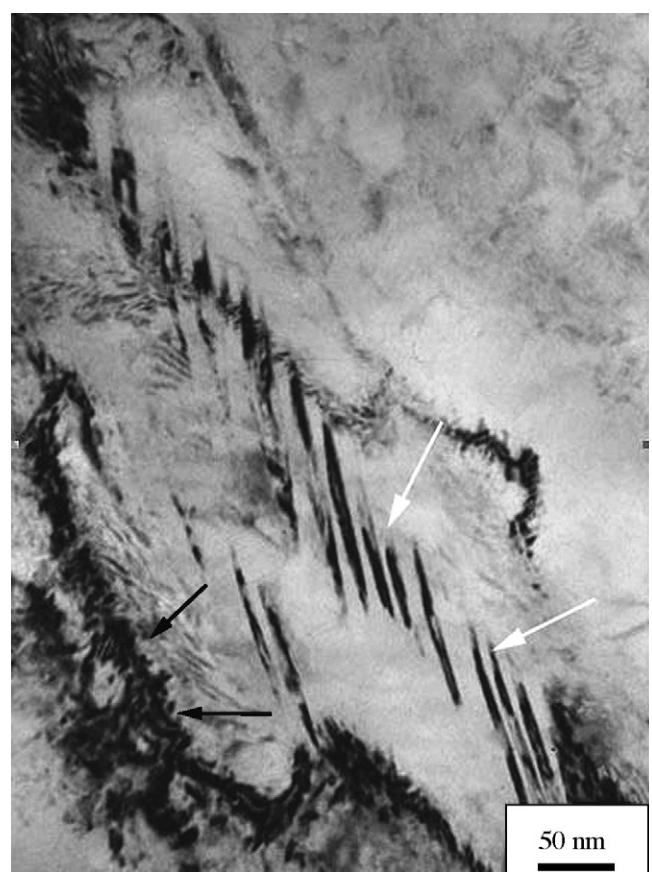

Fig. 5. TEM image of the specimen rolled by 80%.

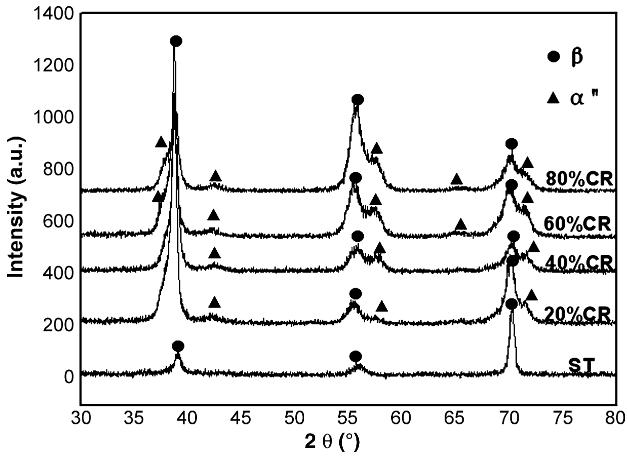

Fig. 6. X-ray diffraction profiles of the solution-treated (ST) and cold-rolled (CR) specimens.

twins. In addition, dislocations tangle was also observed in 80% rolled specimen, which was indicated by black arrows.

3.2. Phase transformation

Fig. 6 shows the X-ray diffraction profiles of the specimens at solid solution-treated and cold-rolled state. As shown in Fig. 6, reflections from β (bcc) single phase were identified by XRD

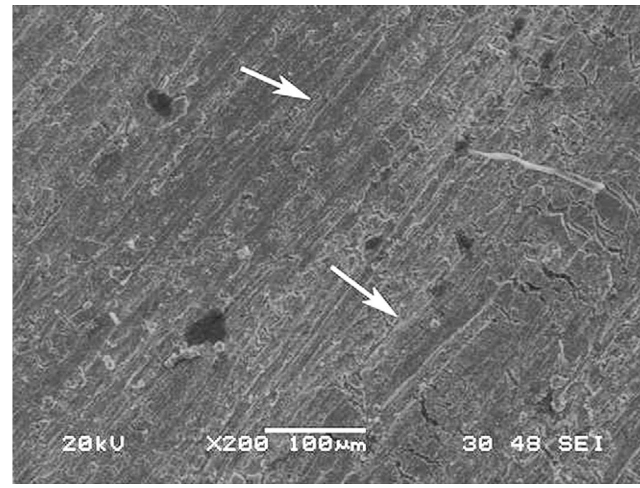

Fig. 8. SEM image of the fracture surface of solution-treated tensile tested specimen.

for solution-treated specimen. While β and α″ (orthorhombic) martensite phases could be observed when the alloy was rolled. With the increase of cold rolling reduction, strain-induced α″ martensite transformation from β to α″ occurred, the reflections of α″-phase increased and the peak intensity rate of α″ to β was to increase. The XRD profiles indicated that with the

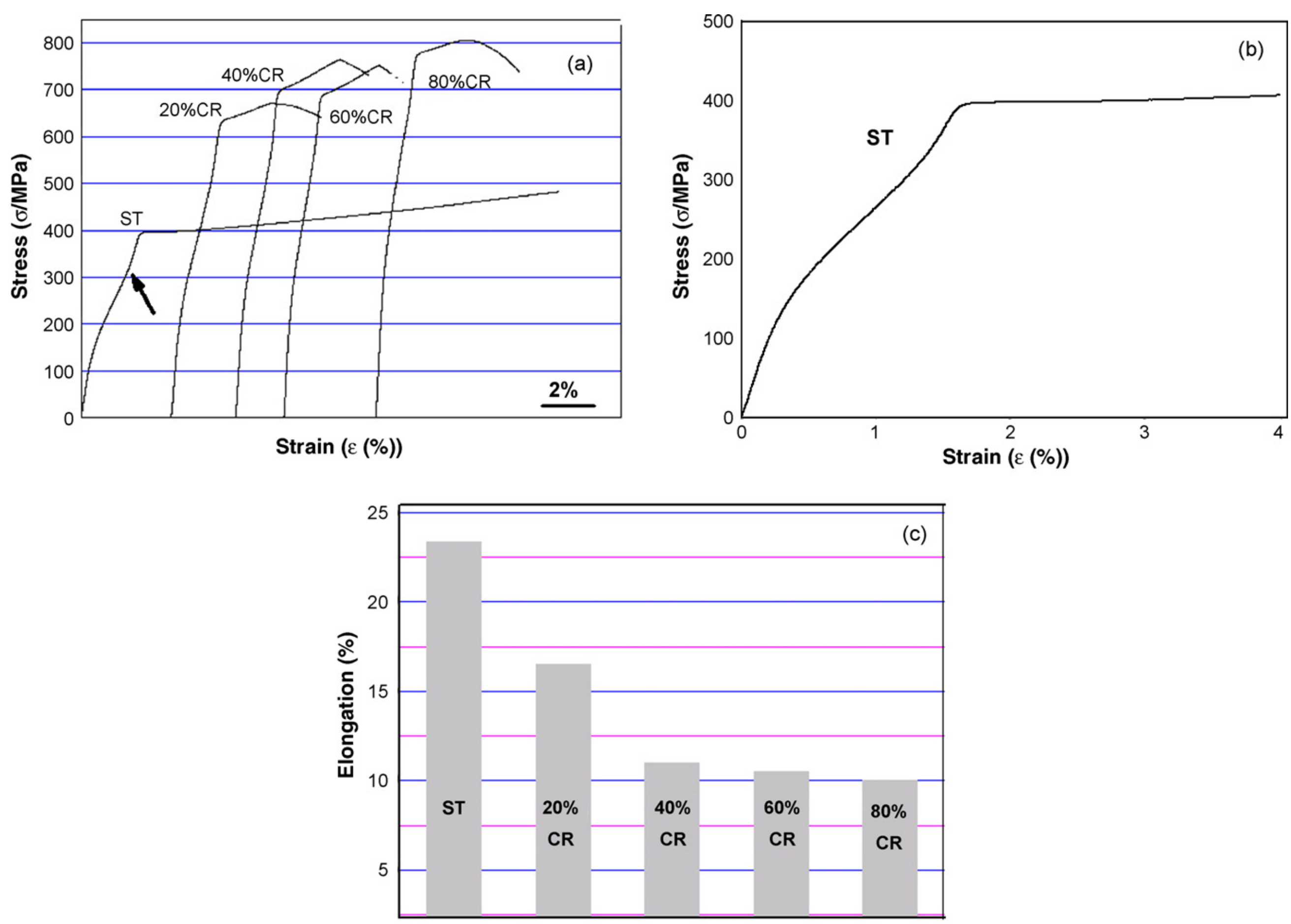

Fig. 7. Stress–strain curves (a and b) and elongation to fracture (c) of specimens treated by solution (ST) and cold rolling (CR).

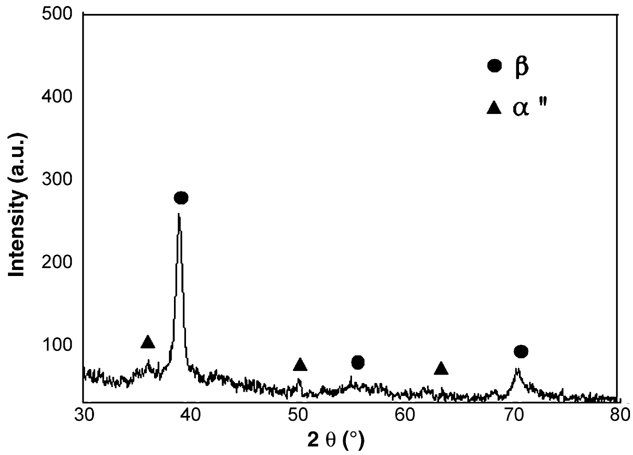

Fig. 9. X-ray diffraction profile of the fracture surface of solution-treated tensile tested specimen.

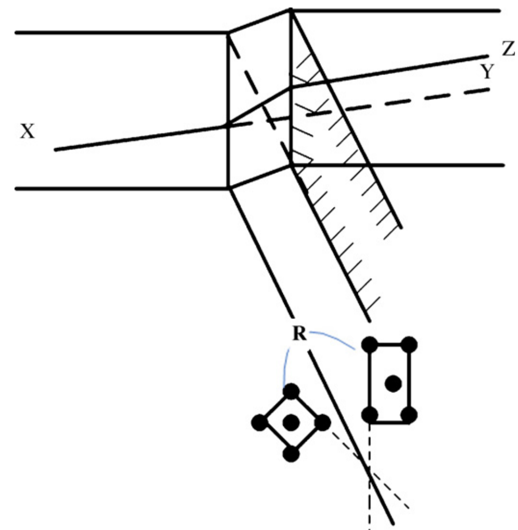

Fig. 10. Sketch map of drape-shaped martensite surface caused by macroscopical shear deformation. *R*: the strain of lattices.

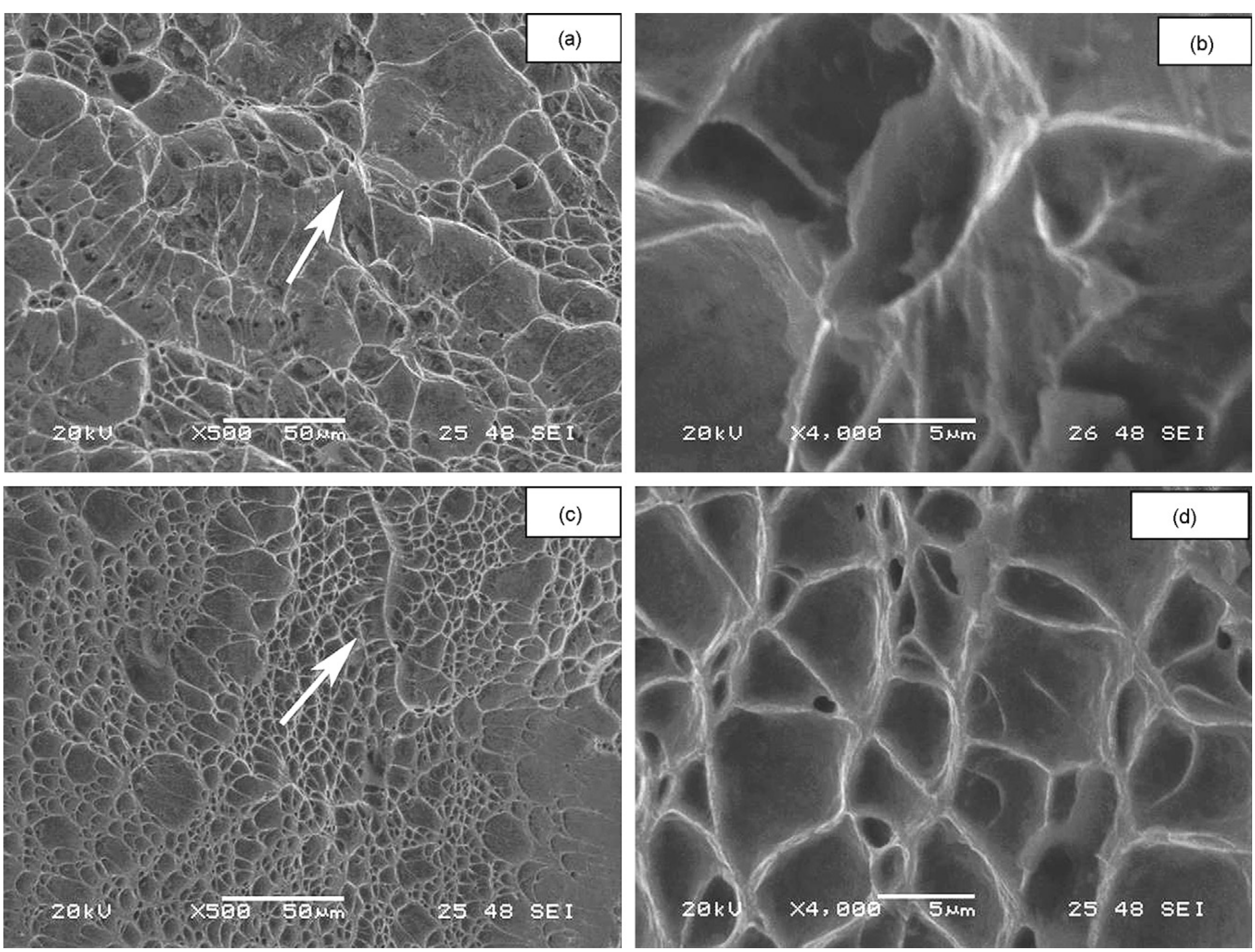

Fig. 11. (a and c) Low-magnification and (b and d) high-magnification SEM images of the fracture surface of 20% (a and b) and 80% (c and d) tensile tested specimens.

increase of reduction, strain-induced martensite transformation was enhanced. Because of residual stress caused by cold rolling, the broad of XRD profiles broadened gradually. Comparing with the specimen treated by solid solution (ST) and the specimen rolled by 80% reduction, much more martensite transformation had been finished, as studied above.

3.3. Mechanical properties

Fig. 7 shows the stress–strain curves (a and b) and elongation to fracture (c) of specimens treated by solution (ST) and cold rolling (CR). The specimen annealed at the temperature of 1053 K for 30 min exhibited a two-stage yielding, as it was shown in Fig. 7(b). The first yielding occurring at around 200 MPa during tensile tests was a relative flat plateau, which was related to the shape memory property of the alloy. The first yield in ST is caused by stress-induced martensite transformation, the second yield would be associated with initiation of slip deformation of α'' martensite. The tensile strength of the specimen treated by solution was around 500 MPa and the elongation to fracture was over 23%, which showed excellent plasticity. As for fracture surface of solution-treated tensile tested specimen, drape-shaped martensite was investigated by SEM analysis, as the arrows show (Fig. 8). X-ray diffraction profile of the fracture surface indicated that stress-induced α'' martensite transformation occurred (Fig. 9). Fig. 10 shows the sketch map of drape-shaped martensite surface caused by macroscopical shear deformation. The macroscopical structure of fracture surface changed from *XY* plane to *XZ* plane, which was attributed to the strain of lattices (R) caused by tensile stress.

Tensile strength increased with the increasing of reduction of cold rolling. Besides dislocations caused during deformation, secondary microstructure of martensite such as twins contributed much to the strength of the alloy [16]. As seen in Fig. 1(e) of the optical microstructure of strain-induced martensite transformation, fibriform and cross-hatched martensite phases appeared in specimen which was rolled with the reductions of 80%. Owing to the fibriform martensite, the tensile strength of the alloy increased. When the reduction added up to 80%, the tensile strength increased to 800 MPa. Elongation to fracture decreased with the increase of reduction of cold rolling shown in Fig. 7(c). As it was known, the plasticity of martensite depends much on the secondary microstructure of martensite. Twins, as the major secondary microstructure of martensite in Ti–Nb–Ta–Zr alloy (Fig. 5), played an important role on the plasticity. The elongation was higher than 15% when the reduction was 20%, which induced bunchy martensite. Comparing with the 20% rolled specimen, when the reduction of cold deformation increased to 40%, the elongation decreased rapidly. However, when the reduction was between 40% and 80%, the elongation decreased gradually. Even when the alloy was deformed by 80% in thickness, the elongation was over 10%, which showed favorable plasticity.

Fig. 11 displays SEM images of the fracture surface of 20% and 80% tensile tested specimens. The fracture morphologies mainly exhibited toughness fracture in both the specimens. The alloy tolerated a large amount of elongation before failure occurred. As seen in Fig. 7(c), elongation to fracture was over 10% even when the alloy was rolled by 80% reduction in thickness. Whirlpool-like patterns were somewhat different due to the reductions of cold rolling. Owing to better plasticity of fracture of the specimen deformed by 20%, fracture morphologies of whirlpool-like patterns were much deeper, seen from high-magnification SEM images in Fig. 11(b). In the correct position of which the arrows show (Fig. 11(b) and (d)), the differences could be observed easily. Moreover, a few cleavage planes appeared in the fracture surface of the specimens deformed by 80%.

4. Conclusions

Strain-induced martensite transformation from β to α'' caused by cold rolling was observed. Mechanical properties of the alloy fabricated by cold rolling were measured. The main results are summarized as follows.

The biomedical titanium alloy of Ti–Nb–Ta–Zr shows excellent cold workability. Different kinds of microstructure of strain-induced martensite are observed during cold rolling. With the increase of reduction of cold rolling, much more strain-induced martensite transformation from β to α'' can be investigated. Microstructure of α'' changes from acicular martensite to butterfly shaped martensite and shows variant crossed and cross-hatched when the reduction of cold rolling was over 60%. The two-stage yielding was observed from stress–strain curves, which shows that stress-induced phase transformation occurs in the alloy treated by solid solution. The tensile strength of the alloy increases with the increasing of the reduction of cold rolling. When the reduction is 80%, the tensile strength increases to 800 MPa and the elongation to fracture is over 10%. Ti–Nb–Ta–Zr exhibits high strength and appropriate plasticity when it is cold-rolled by 80% reduction in thickness, which contributes much to medical applications.

Acknowledgements

We would like to acknowledge a financial support provided by High Technology Research and Development Program of China under Grant No.: 2006AA03Z559, 973 Program under Grant No.: 2007CB613806. A Foundation for the Author of National Excellent Doctoral Dissertation of PR China under Grant No.: 200332.

References

[1] T.W. Duerig, J. Albrecht, D. Richter, P. Fischer, Acta Metall. 30 (1982) 2161–2172.
[2] E. Takahashi, T. Sakurai, S. Watanabe, N. Masahashi, S. Hanada, Mater. Trans. 43 (2002) 2978–2983.
[3] J.I. Kim, H.Y. Kim, T. Inamura, H. Hosoda, S. Miyazaki, Mater. Sci. Eng. A 403 (2005) 334–339.
[4] H. Kawahara, Bull. Jpn. Met. 31 (12) (1992) 1033–1039.
[5] M.R. Krigman, A.P. Silverman, Neurotoxicology 5 (2) (1984) 129–139.
[6] K.A. Winship, Adverse Drug React. Acute Poisoning Rev. 1 (1988) 19–38.
[7] S.G. Schafer, U. Femfert, Regul. Toxicol. Pharmacol. 4 (1984) 57–69.
[8] G.J. Yang, T. Zhang, J. Alloy Compd. 92 (2005) 291–294.
[9] H.Y. Kim, T. Sasaki, K. Okutsu, et al., Acta Mater. 54 (2006) 423–433.

[10] M. Morinaga, N. Yukawa, in: M. Doyama et al. (Ed.), "Alloy Design Base on Molecular Orbital Method" Computer Aided Innovation of New Materials, Amsterdam: North-Holland, 1991, pp. 803–808.

[11] A.A. Ilyin, M.Y. Kollerov, I.S. Golovin, J. Alloy Compd. 253/254 (1997) 144–147.

[12] P.L. Ferrandini, F.F. Cardoso, S.A. Souza, C.R. Afonso, R. Caram, J. Alloy Compd. 433 (2007) 207–210.

[13] T. Saito, T. Furuta, J.H. Hwang, S. Kuramoto, K. Nishino, N. Suzuki, et al., Science 300 (2003) 464–467.

[14] S.Q. Chen, Metallography of Titanium Alloy, National Defense Industry Press, Beijing, 1986.

[15] P. Laheurte, A. Eberhardt, M.J. Philippe, Mater. Sci. Eng. A 396 (2005) 223–230.

[16] H.C. Lin, S.K. Wu, T.S. Chou, H.P. Kao, Acta Metall. 39 (1991) 2069–2080.